Crack Propagation Prediction in Aluminum Friction Welded Joints

BROŽ Petr[1,a] and DOBIÁŠ Daniel[2,b]

[1]University of West Bohemia, Faculty of Applied Sciences, Univerzitní 8, 306 14 Pilsen, Czech Republic

[2]Czech Technical University in Prague, Klokner Institute, Šolínova 7, 166 08 Prague 6, Czech Republic

[a]broz.petr@tiscali.cz, [b]dobias@klok.cvut.cz

Introduction

The friction welding procedure to achieve lightweight structures proved to be of great importance and the practical prediction of fatigue performance of weldments is a principal element.

In the treatise, in conformity with [1] methodology, an integrated dual boundary element method – finite element method (DBEM – FEM) technique, coupling the welding procedure simulation to the successive crack propagation evaluation, is presented and applied to model multiple crack growth. The friction butt of the precipitation hardened AA 2024 – T3 alloy has been simulated employing a thermo – mechanical FEM model to predict the process caused residual stress field and material softening. The computed stress field is transferred to a DBEM environment and superimposed to the stress field caused by a remote fatigue tensile load applied on a notched specimen. The entire procedure is tried out comparing simulation results with experimental data. The agreement obtained emphasized the predictive of the technique. It has been also analyzed the effect of the residual stress distribution on crack propagation and the interaction between growing cracks.

Owing to wide structural application in the various industries, the aluminum alloy AA 2024 – T3 was chosen as base material. Particularly, the thermo – mechanical FEM model, according to [2] was employed to determine the residual stress state in the butt welded aluminum plates. Further, multiple crack propagation was simulated by the DBEM. The influence of residual stresses on crack growth rates was modeled by the crack growth law in accordance with [3], [4].

DBEM – FEM representation

In thermo – mechanical modeling of friction welding, the most familiar assumption, used to make smaller the computational complexity, is to ignore the material flow in course of welding. This brings about semi – coupled thermo – mechanical models in a Lagrangian formulation where the thermal field is analyzed prior to the mechanical field by separating out the two analyses. The model applied was presented by Sonne at al. [2] The time dependent temperature classification was derived by analyzing the transient heat conduction equation, that is

$$\rho c_p \frac{\partial T}{\partial t} = \frac{\partial T}{\partial x}\left(k\frac{\partial T}{\partial x}\right) + \frac{\partial T}{\partial y}\left(k\frac{\partial T}{\partial y}\right) + \frac{\partial T}{\partial z}\left(k\frac{\partial T}{\partial z}\right) + \dot{Q}'''_{gen}$$

(1)

where ρ is the material density, c_p is the specific heat capacity, T is the temperature, k is the thermal conductivity and Q_{gen} is the volumetric heat source term. The tool operation is

modeled through proper boundary condition applied at the interface between the shoulder and the work piece. A surface heat flux q dependent on the radial place and the local yield stress σ_{yield}, is imposed at the tool shoulder – adjacent material contact area, without modeling the tool sensor, like this

$$q(r,T) = \left(\frac{2\pi n}{60}\right) r \frac{\sigma_{yield}}{\sqrt{3}},$$

(2)

where π is the number of tool revolutions per minute, r is the radial position going from the tool center out, and σ_{yield} is the temperature dependent yield stress.

The progress of microstructure of the Al – alloys 2024 in the T3 temper state in the course of friction welding has been demonstrated to possess a significant influence on the residual stress distribution. In this article, the softening model developed by Myhr and Grong was employed to predict the phase transformation during welding. The same approach was also adopted by Richards et al. The model relates the fraction of dissolved hardening precipitates X_d to the equivalent time of heat treatment $t_{eq} = t/t^*$ (where t is the period of time at a temperature T and t^* is the time for total precipitate dissolution at this temperature) in the following manner:

$$\frac{f}{f_0} = 1 - X_d = 1 - t_{eq}^n = 1 - \sqrt{t_{eq}}$$

(3)

$$t_{eq} = \sum_{i=1}^{N_{total}} \frac{\Delta t_i}{t_i^*} = \sum_{i=1}^{N_{total}} \frac{\Delta t_i}{t_{ref} \, exp\left[\frac{Q_{eff}}{R}\left(\frac{1}{T_i} - \frac{1}{T_{ref}}\right)\right]}$$

(4)

where t_{ref} is the time for total dissolution at the reference temperature $T_{ref,}$, R is the universal gas constant and Q_{eff} is the effective energy for precipitate dissolution. The small piece of hardening precipitates f/f_0 to the equivalent time via the fraction of dissolved precipitates X_d as demonstrated in Eq. (3), where n is a material constant. The yield stress was predicted through a linear interpolation between the first and entirely dissolved states.

To calculate the transient likewise the residual stress field in the work piece, a normal mechanical model based on the solution of the three static force equilibrium equations is applied, that is

$$\sigma_{ij,j} + p_j = 0$$

(5)

where p_j is the body force at any point within the plate and σ_{ij} the stress tensor. Hooke´s generalized law and linear decomposition of the strain tensor, as well as small strain theory, were applied together with the expression for the thermal strain. The plastic strain evolution is based on the standard J_2 flow theory with a temperature dependent von Mises yield surface. According to [2], isotropic hardening behavior is the most suitable for modeling the mechanical behavior of AA2024 – T3 when combined with a softening model. The yield stress at the instantaneous temperature was determined by interpolating between the upper and lower bound yield stress curves relative to X_d, ie:

$$\sigma_y = \left(\sigma_{y_{max}} - \sigma_{y_{min}}\right)\frac{f}{f_0} + \sigma_{y_{min}}$$

(6)

where σ_{max} is the yield stress of the material in the original T3 condition and σ_{min} the yield stress of the in full dissolved material. The upper and lower yield stress curves for AA2024 – T3 are available in [2]. The Vickers microhardness (HV) distribution was calculated by

acquiring the same model as in Eq. (6), evidently substituting yield stress with microhardness values, as follows

$$HV = (HV_{max} - HV_{min})\frac{f}{f_0} + HV_{min}$$

(7)

using the minimum and maximum hardness values calibrated on the experimental data.

Crack growth model using DBEM

The residual stresses put on in the main and lateral crack surfaces were imported in the commercial kit BEASY for the DBEM growth analysis. An interface procedure already available in the BEASY environment was used for this purpose. The propagation was driven by the remote fatigue load and by the superimposed residual stress field (applied on the crack faces). At each step of propagation, new meshed surfaces were automatically added to the previous crack configuration, consistent with the outcomes of the implemented crack growth law. Again the interface routine scanned the .odb file to extract the residual stress to be applied in addition to the residual stresses already existing on the previous crack surface. Then the remote load was applied again and a new LEFM analysis was performed in an interactive procedure that stopped when a predefined instability crack condition was encountered, i.e. when the stress intensity factor at the crack front reaches a critical value. There is demonstrated in Fig. 1 a block diagram clarified the general routine.
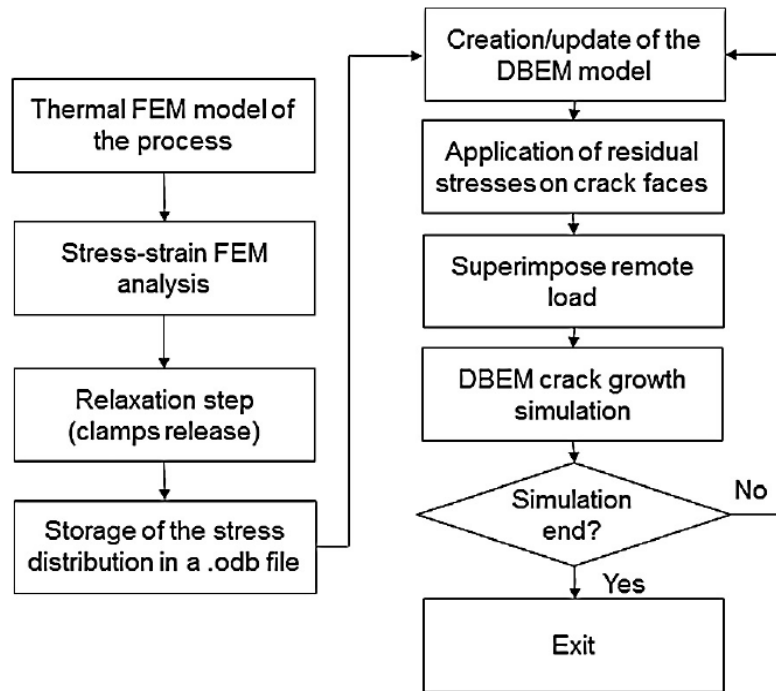

Fig. 1, Block diagram of the executed DBEM – FEM model [1]

Residual stresses influence crack growth because they modify the effective value of the total stress intensity factor at the crack tip, with both the minimum (K_{min}) and the maximum (K_{max}) values in general being alike influenced, going away the parameter $\Delta K = K_{max} - K_{min}$ unchanged. Consequently, the primary effects of residual stresses on crack growth rates are related to the K_{max} variations rather than to the ΔK variations. This is accounted for by a two – parameter approach. According to this, fatigue crack growth is promoted by two driving forces, K_{max} and ΔK. In addition, the procedure assumes that there are two fatigue thresholds $K^*_{max,th}$ and ΔK^*_{th} corresponding to the two driving forces both of which must be

simultaneously larger than the relative thresholds for fatigue crack growth to occur. The crack propagation law is expressed by the ensuing manner:

$$\frac{da}{dN} = A\left(\Delta K - \Delta K_{th}^*\right)^n \left(K_{max} - K_{max,th}^*\right)^m$$

(8)

At the same time eq (8) was stamped by best fitting the material parameters *A, n, m* based on literature data. The following values were used for the parameters: $\Delta K_{th}^* = 1,834,121$ N/m$^{3/2}$, $K_{max,th}^* = 3,352,014$ N/m$^{3/2}$, $A = 6.745E-23$ m$^{1.5(n+m)+1}$/N^{n+m}, $n = 1.65$, $m = 0.56$. These parameters are valid for each positive *R* ratio ($\sigma_{min}/\sigma_{max} = K_{min}/K_{max} > 0$). The effects of friction stir welding were emulated by taking into account the residual stress influence on the driving parameters *ΔK* and K_{max}. Hence, the SIFs used in Eq. (8) were computed as the sum of the SIF corresponding to the remote load and that of the SIF corresponding to process induced residual stresses. In the DBEM analysis, residual stresses were simulated by employing a distribution of tractions on the crack faces checked with the residual stresses caused by the welding method.

Experiments

AA2024-T3 aluminum rolled sheets were connected by friction welds applying a non – consumable Cr – Mo steel tool, adopting an angular tool velocity of 1400 rpm and a welding speed of 70 mm/min. The geometry was characterized by a flat shoulder (20 mm in diameter) with an unthreaded conical pin (6.2 mm in major diameter, a cone angle of 30°and a height of 3.8 mm). The forging action of the tool shoulder was enhanced by imposing a tilt angle of 2°. The dimensions of the adjoining sheets were 200 mm (length), 30 mm (width), and 4 mm (thickness). The welding configuration is indicated in Fig. 2.
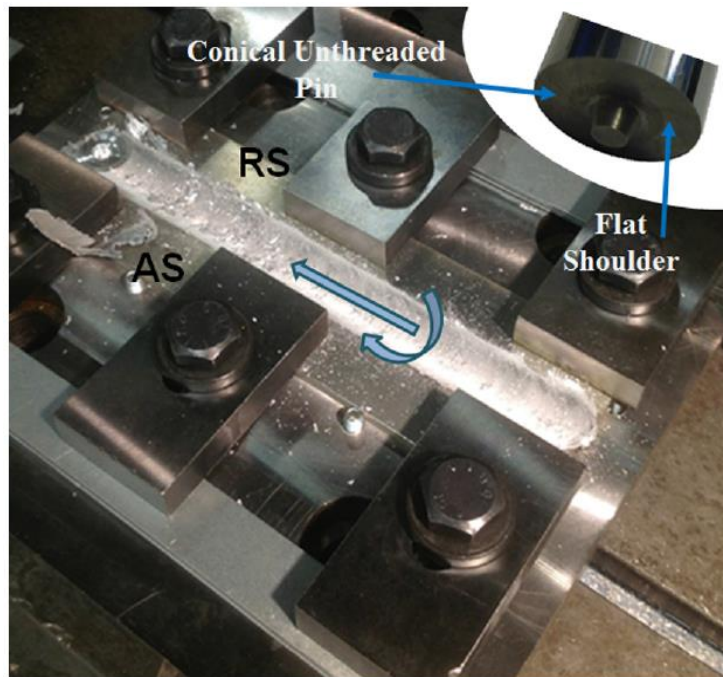

Fig. 2, Welding arrangement

The longitudinal residual stress classification in the not specific section of the welded joint was gained by dint of the contour method. The resulting stress field was already used for crack propagation assessment by some authors, assuming the repetition of the stress field as

computed at the mid – length in each cross section orthogonal to the weld line. However, the outlined hybrid (numerical – experimental) method is obviously quite expensive and not generalizable, since the stress analysis is case specific, calling for a repetition of the procedure for each variation of processing parameters and conditions. What is more, accounting for transient effects and stress relaxation in the proximity of the free edges of the sheets was not provided in the crack growth simulations. In that sense, the model in this work stands for a generalization of the algorithm because the residual stresses are predicted numerically taking the different boundary conditions likewise stress relaxation into consideration.

The sensitivity of the model with respect to variations in material properties was assessed by comparing the numerically estimated and experimentally measured microhardness along a line orthogonal to the weld line at the mid – thickness of the specimen. Vickers microhardness was measured using an automatic device applying the following test parameters: indentation load 100gf (0.98 N), loading time 15 s, and indentation speed 60μm/s. the distance between two consecutive indentations was defined as 1 mm. The analysis was performed after 60days of (post welding) natural aging to ensure the establishment of a stable microstructure.

Model validity

Experimental data are got by the contour method. The first part of an appropriate thermo – mechanical model is to possess a realistic account of the temperature field before the follow – up mechanical analysis. Certainly, temperature gradients are both the direct and indirect sources for stresses in view of thermal expansion and metallurgical changes in the aluminum. The transient temperature field during welding (Fig. 3a), stipulated by the thermal computation, is employed in the subsequent stress analysis to get the stress state progress in the welded plate. In Fig. 3b the typical lines in compression at the sides of the moving heat source and in tension then behind the moving heat source can be studied as an outcome of the self – constraining influence acted by the colder neighbouring material.
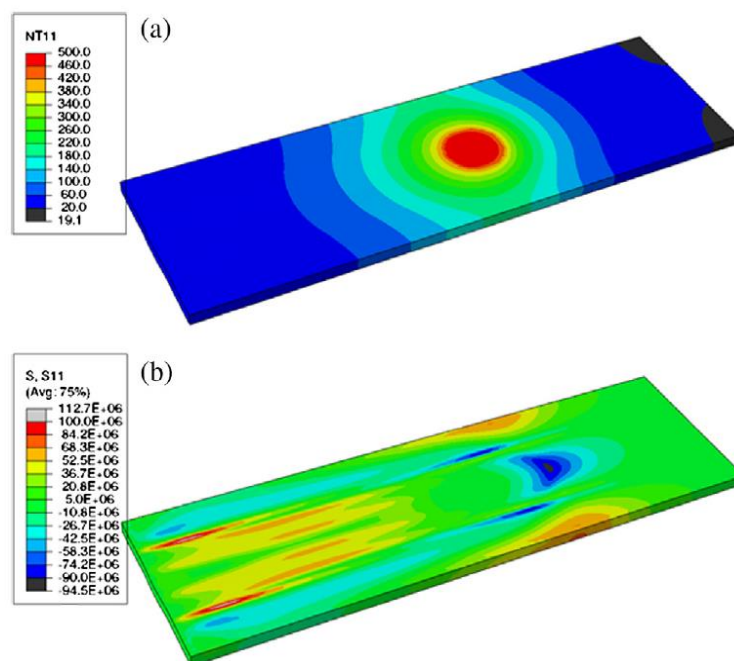

Fig. 3 (a) Temperature field (°C) from the heat transfer study of welding at $t = 100$ s. (b) The resultant longitudinal stress constituent (N/m^2) from the stress study at the same step [1]

In the friction welding method, heat is set up by the friction between the tool shoulder and the work piece surface, and by the plastic deformation induced in the work piece. The material under and right next to the tool is heated up resulting in expansion; however it is partly constrained by the relatively colder material surrounding this region. Subsequently, the material starts yielding in compression and plastic deformation starts to develop. Besides, the thermal gradients due to non – uniform heat generation and the mechanical boundary conditions (i.e. clamping, contact conditions between work piece and the anvil etc.) also play a significant role for promoting plastic strains and consequently considerable role for publicized plastic strains and accordingly residual stresses.

Crack growth

A multiple crack growth was demonstrated by tests and it was marked by the appearance of the aforesaid lateral crack created from a notch insincerely introduced after the welding process and of a central semi - elliptic crack, it itself nucleated in the weld crown owing to the surface marks left by the tool shoulder. The basic hypothesis, to be verified by the simulations, is that, in the initial phase of the fatigue test, the central crack, due to its reduced size and to the distance from the lateral crack, does not significantly influence the propagation of the lateral crack itself. In this link it should be remarked that in the experiments, the lateral crack, starting from the notch tip, was considered initiated after a pre – cracking phase lasting a number of cycles sufficient to prolong the notch by nucleation of a crack whose superficial length is equal to 0.25 mm. Hence, the initial single crack simulated scenario was based on a lateral through crack with an overall length (2.25 mm) equal to the sum of notch length (2 mm) and pre – crack length (0.25 mm). Taking into consideration that the nucleation time and dimension of central crack were not known a priori and in view of the absence of experimental indication, up to this period, any interaction between the two cracks, the central crack was presupposed small and accordingly not modeled at all in the thought over original crack growth stage.

Eg., to demonstrate the matter investigated, the lateral crack was extended to simulate in a single crack growth, up to 2.5 mm length, before brought in the second central crack in the model. The timing for the introduction of the central crack in the numerical model was prescribed by the experimental watching, as follows: when the lateral crack achieved 2.5 mm in length it is subject to sudden acceleration uncovered and shown by the applied gauges.
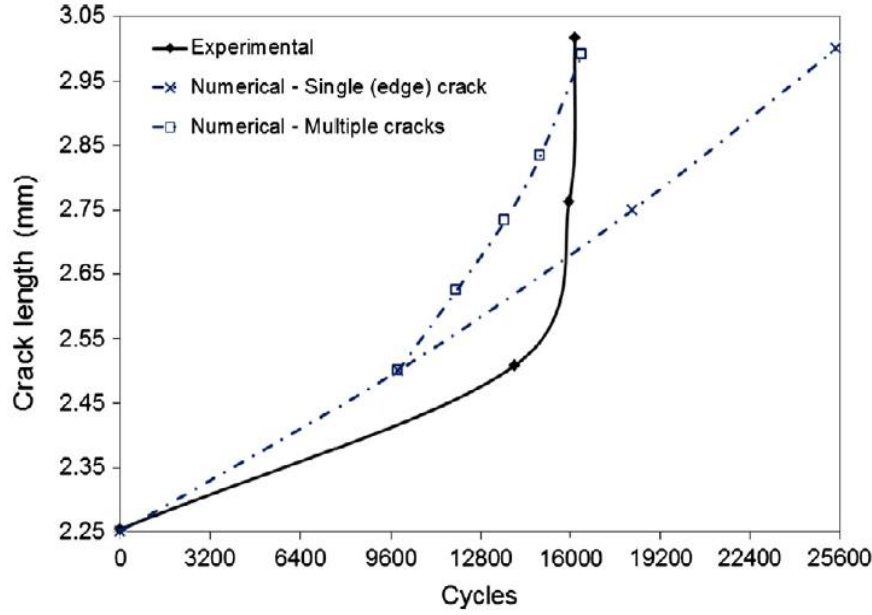
Fig. 4, Lateral crack length experimentally checked and calculated by DBE supposing single crack growth (without central crack) and multiple crack growth (introducing an additional central crack after nearly 10 000 cycles)

The central crack growth proved to be accountable for specimen failure, with connected K_I values (mote II and III are nearly inconsiderable) approaching the material fracture toughness. On the other hand, SIFs along the lateral crack front, according to the J – integral were not adequately high in comparison with the threshold ($K_{max,\ th}$ = 3.352 Pa.m$^{0.5}$) to produce perceptible crack forward movements (Fig. 5).
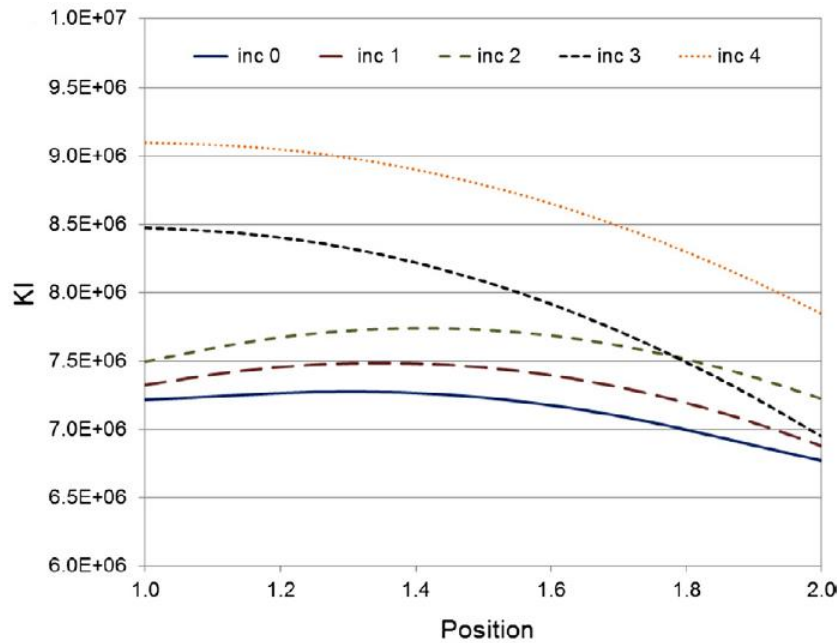

Fig. 5, SIF values (Pa m$^{0.5}$) alongside the crack fronts of the two cracks for each simulation increment (inc 0-9850 cycles; inc 1-1,920 cycles; inc 2-13,660 cycles; inc 3-14,920 cycles; inc 4-16,400 cycles); of crack growth: the coordinate from 1 to 2 relates to crack 1 [1]

Conclusions

Some deductions can be emphasized:

- the realized DBEM – FEM way of tackling proof to be able to efficiently predict multiple crack propagation in the presence of residual stresses
- the crack growth stipulated by the experiment, as conceived by post examination metallographic analyses, was worked by a nearly pure mode I evolution and nearly symmetric form. This finding served as a qualitative corroboration of the residual stress field determined by numerical simulation.
- if the initial crack sets out from the weld line, the process induces opening stresses having an accelerating influence on the crack growth

Acknowledgment

References

[1] R. Citerella, P. Carlone, M. Lepore, GS. Palazzo, Numerical – experimental crack growth analysis in AA2024-T3 FSWed butt joints. Adv Eng Softw 2015; 80: 47-57.

[2] M.R. Sonne, C.C. Tutum, J.H. Hattel, A. Simar, B. deMeester, The effect hardening laws and thermal softening on modeling residual stresses in FSW of aluminium alloy 2024-T3, J Mater Process Technol 2013; 213:477-86.

[3] P. Carlone, R. Citarella, M. Lepore, G.S. Palazzo, A FEM-DBEM investigation of the influence of process parameters on crack growth in aluminium friction stir welded butt joints, Int J Mater Form 2015; 8(4):591-9.

[4] P. Brož, D. Dobiáš, Important Aspects of Testing Welds, EAN 2017, Nový Smokovec (2017), pp 185-186.